The Astrophysical Journal Letters, 778:L1 (5pp), 2013 November 20 doi:10.1088/2041-8205/778/1/L1

LABORATORY MEASUREMENTS AND TENTATIVE ASTRONOMICAL IDENTIFICATION OF H_2NCO^+

H. Gupta[1,3], C. A. Gottlieb[2], V. Lattanzi[2,4], J. C. Pearson[1], and M. C. McCarthy[2]
[1] Jet Propulsion Laboratory, California Institute of Technology, 4800 Oak Grove Drive, Pasadena, CA 91109, USA
[2] Harvard-Smithsonian Center for Astrophysics, 60 Garden Street, Cambridge, MA 02138, USA
Received 2013 July 30; accepted 2013 September 11; published 2013 October 30

ABSTRACT

The rotational spectrum of H_2NCO^+, the ground-state isomer of protonated HNCO, has been measured in a molecular beam in the centimeter band with a Fourier transform microwave spectrometer and in a low-pressure laboratory discharge in absorption in the millimeter band. Spectroscopic constants, including the nitrogen–14 hyperfine coupling constant, derived from 30 *a*-type transitions between 20 and 367 GHz with $J \leqslant 18$ and $K_a \leqslant 3$ allow the principal rotational transitions to be calculated to 1 km s^{-1} or better in equivalent radial velocity well into the far IR. Two low-lying rotational transitions of H_2NCO^+ in the centimeter band ($0_{0,0}$–$1_{0,1}$ and $1_{1,0}$–$2_{1,1}$) were tentatively identified in absorption in the PRIMOS spectral line survey of Sgr B2(N) with the Green Bank Telescope. The lines of H_2NCO^+ arise in a region of the Sgr B2(N) halo whose density is low ($n < 1 \times 10^4$ cm^{-3}). The derived column density of (6–14) $\times$ 10^{11} cm^{-2} implies that the fractional abundance is $\sim$10^{-12}. Owing to the ubiquity of HNCO in galactic molecular clouds, H_2NCO^+ is a good candidate for detection in sources spanning a wide range of physical conditions.

Key word: ISM: molecules

Online-only material: color figure

1. INTRODUCTION

Isocyanic acid (HNCO)—the simplest molecule composed of the elements H, C, N, and O—was one of the first polyatomic molecules identified in the interstellar gas (Snyder & Buhl 1972). Over the intervening years, it has been observed in over 60 galactic sources including diffuse, translucent, and cold dark clouds; high-mass star-forming regions (Martín et al. 2008); and nine external galaxies (Martín et al. 2009). More recently, cyanic acid (HOCN), the lowest metastable isomer of HNCO, 12,400 K higher in energy, was detected in some of the same sources in which HNCO is observed (Brünken et al. 2009, 2010). But unlike the example of HCN and HNC (see Hirota et al. 1998, and references therein), the HNCO/HOCN ratio of 50–600 is much greater than unity in both cold and warm interstellar clouds (Marcelino et al. 2010; Brünken et al. 2010). Because the formation of HNCO and its isomers is still not fully understood, observations of the ionic precursors of HNCO and HOCN might help identify the pathways that result in the observed HNCO/HOCN ratio. However, prior to this work the rotational spectrum of protonated HNCO had not been measured in the laboratory.

There are two main isomers of protonated HNCO: the planar symmetric ground-state H_2NCO^+, and the bent chain $HNCOH^+$ about 9050 K higher in energy (Lattanzi et al. 2012). Both are isoelectronic and similar in structure and relative stability to ketene (H_2CCO) and its isomer ethynol (HCCOH; Green 1981). Dissociative recombination of H_2NCO^+ was first mentioned as a possible source of HNCO in the cold dark cloud TMC-1 more than 30 yr ago (Brown 1981). Recently, chemical models have included H_2NCO^+ in the gas phase synthesis of HNCO (Tideswell et al. 2010; Quan et al. 2010). Because $HNCOH^+$ can yield HNCO and HOCN, the analogy with HCN/HNC suggests that $HNCOH^+$ rather than H_2NCO^+ might be the precursor of HNCO (Lattanzi et al. 2012). However, the large observed HNCO/HOCN ratio implies that H_2NCO^+ might instead be the main precursor (Adande et al. 2010). In the absence of laboratory data on the gas-phase reactions of H_2NCO^+ and $HNCOH^+$, direct astronomical observations might help elucidate the synthesis of HNCO and HOCN in space. Both ions are excellent candidates for radio astronomical detection, owing to the substantial dipole moments (4.13 D for H_2NCO^+ and 1.3 D for $HNCOH^+$; Lattanzi et al. 2012) and favorable rotational partition functions.

A preliminary account of the laboratory detection of the lowest rotational transitions of H_2NCO^+ and $HNCOH^+$ in the centimeter band was recently reported by Lattanzi et al. (2012). Here we present a full account of the laboratory measurements of H_2NCO^+ in the millimeter band, and the characterization of its spectrum to high accuracy well into the far IR. We also discuss the tentative identification of two transitions in the centimeter band in absorption toward Sgr B2(N)—the well known hot core in the giant molecular cloud (GMC) in Sagittarius.

2. LABORATORY MEASUREMENTS OF H_2NCO^+

The rotational spectrum of H_2NCO^+ in the millimeter band was measured in a free space glow discharge spectrometer used to detect many reactive species of astronomical interest including carbon chain radicals, carbenes, and negative molecular ions (Gottlieb et al. 2003). The search for lines of H_2NCO^+ in the millimeter band was guided by rotational constants derived from measurements of three rotational transitions in the centimeter band observed in a supersonic beam, and fourth-order centrifugal distortion constants calculated theoretically (Lattanzi et al. 2012). In all, more than 15 rotational lines between 222 and 367 GHz were measured to high accuracy (Table 1). Lines of H_2NCO^+ were most intense in a DC glow discharge through a flowing mixture of HNCO and H_2 in the molar ratio 2:1,

[3] Current address: Infrared Processing and Analysis Center, California Institute of Technology, 770 S. Wilson Avenue, Pasadena, CA 91125, USA
[4] Current address: Observatoire de Paris, 61 Avenue de l'Observatoire, F-75014 Paris, France.

Table 1
Laboratory Frequencies of H_2NCO^+

Transition[a] $J'_{K'_a,K'_c}$–J_{K_a,K_c}	F'–F	Frequency (MHz)	$O-C$[b] (kHz)
$1_{0,1}$–$0_{0,0}$	0–1	20225.977(5)	4
	2–1	20227.417(5)	2
	1–1	20228.378(5)	0
$2_{1,2}$–$1_{1,1}$	1–1	40122.510(5)	−2
	3–2	40123.542(5)	3
	2–1	40124.596(5)	5
	2–2	40124.873(5)	−3
$2_{0,2}$–$1_{0,1}$	1–1	40453.209(5)	−1
	3–2	40454.751(5)	5
	2–1	40454.813(5)	−2
	1–0	40455.622(5)	6
	2–2	40455.776(5)	−2
$11_{0,11}$–$10_{0,10}$		222429.163(28)	−37
$12_{0,12}$–$11_{0,11}$		242634.511(21)	−35
$13_{0,13}$–$12_{0,12}$		262835.849(19)	−8
$16_{0,16}$–$15_{0,15}$		323412.242(25)	−21
$16_{3,14}$–$15_{3,13}$		323504.113(35)	−27
$16_{3,13}$–$15_{3,12}$		323505.206(50)	−30
$17_{1,17}$–$16_{1,16}$		340942.497(50)	24
$17_{0,17}$–$16_{0,16}$		343594.160(37)	37
$17_{3,15}$–$16_{3,14}$		343719.214(25)	41
$17_{3,14}$–$16_{3,13}$		343720.624(25)	−36
$17_{2,16}$–$16_{2,15}$		343723.034(45)	−36
$17_{2,15}$–$16_{2,14}$		343936.173(20)	13
$17_{1,16}$–$16_{1,15}$		346542.920(20)	38
$18_{0,18}$–$17_{0,17}$		363770.319(22)	16
$18_{2,17}$–$17_{2,16}$		363929.847(62)	18
$18_{3,15}$–$17_{3,14}$		363935.452(18)	8
$18_{2,16}$–$17_{2,15}$		364182.753(20)	−15
$18_{1,17}$–$17_{1,16}$		366912.602(20)	−27

Notes. Here and in Table 2, the 1σ uncertainties (in parentheses) are in units of the least significant digits.
[a] Levels with odd K_a have *ortho* symmetry and those with even K_a *para* symmetry. Nitrogen–14 quadrupole hyperfine structure is unresolved in the millimeter-wave transitions.
[b] Calculated with the spectroscopic constants in Table 2.

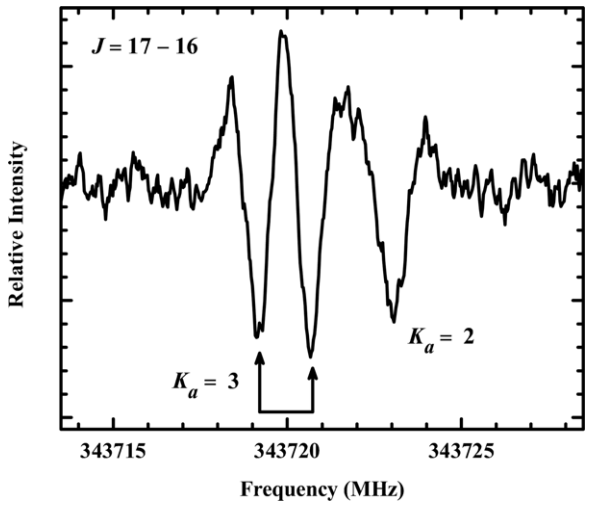

Figure 1. Sample laboratory spectrum of the *ortho* $K_a = 3$ asymmetry doublet and *para* $K_a = 2$ transition of H_2NCO^+ near 343.7 GHz. Owing to the modulation and detection scheme employed, the instrumental line shape is approximately the second derivative of a Lorentzian. The integration time was 13 minutes.

Table 2
Spectroscopic Constants of H_2NCO^+ (in MHz)

Constant	Measured[a] (This Work)	Theoretical[b]	H_2CCO (Ketene)[c]
A	319782(103)	319691	282090
B	10278.6846(26)	10280	10293
C	9948.9034(23)	9952	9916
$10^3 D_J$	3.0677(33)	2.96	3.2824
D_{JK}	0.3775(11)	0.386	0.4779
D_K	25.3[d]	25.3	22.8
$10^6 d_1$	−112(2)	−97	−148
$10^6 d_2$	−38(2)	−26	−58
$10^6 H_{KJ}$	−342(95)	...	−578
χ_{aa}(N)	3.2072(57)	3.218	...
χ_{bb}(N)	0.951(10)	0.929	...

Notes.
[a] Spectroscopic constants derived from a least-squares fit to the transitions in Table 1.
[b] Rotational constants and quadrupole coupling constants calculated at the CCSD(T) level of theory (Lattanzi et al. 2012; S. Thorwirth 2012, private communication).
[c] Constants from Guarnieri & Huckauf (2003, and references therein).
[d] Constrained to the theoretical value.

a discharge current of 100 mA, and a pressure of 15 mtorr with the walls of the absorption cell cooled to 220 K. Under these conditions, the signal-to-noise ratio (S/N) was generally greater than about 10 after 13 minutes of integration (Figure 1).

Quantum calculations predict that H_2NCO^+ is planar with a two-fold symmetry axis parallel to the *a*-inertial axis (Lattanzi et al. 2012). Experimental evidence that H_2NCO^+ has C_{2v} symmetry is provided both by the laboratory and astronomical observations. First, in our cold supersonic molecular beam, the population in the $K_a = 1$ rotational ladder would be too low to observe transitions in this ladder if the lowest *ortho* level ($J_{K_a,K_c} = 1_{1,1}$, 15.8 K above ground) were not metastable. Second, the astronomical observations in Sgr B2(N) provide independent evidence in support for C_{2v} symmetry (see Section 3) by a similar argument as that for the molecular beam.

Nearly harmonic *a*-type rotational transitions, and nitrogen–14 quadrupole hyperfine structure (hfs) in H_2NCO^+ result in a readily identifiable spectrum. On the assumption of C_{2v} structural symmetry, the two H atoms are equivalent and the rotational levels have *ortho* or *para* symmetry with statistical weights of 3:1, analogous to H_2CO (formaldehyde) and several other molecules observed in space. Because radiative and collisional transitions between levels of opposite symmetry are strongly forbidden, *ortho* and *para* H_2NCO^+ are essentially distinct molecules. Hfs from the ^{14}N nucleus with the expected magnitude allowed us to unambiguously assign lines of H_2NCO^+ in the centimeter band both in the supersonic molecular beam and in Sgr B2(N).

A combined analysis of the centimeter- and millimeter-wave rotational transitions of H_2NCO^+ yields highly precise spectroscopic constants. The 30 lines in Table 1 are reproduced with a standard asymmetric rotor Hamiltonian with 10 adjustable constants: three rotation, four fourth-order distortion, one sixth-order distortion, and two quadrupole coupling constants to an rms residual of 22 kHz (i.e., 0.04 km s^{-1} or better at 370 GHz). The measured spectroscopic constants of H_2NCO^+ are comparable to those of the well-studied H_2CCO (ketene) which is similar in size and structure, and to the theoretical constants (see Table 2). Only the *A* rotational constant is not well determined, owing to the well known difficulty in deriving it from $\Delta K_a = 0$

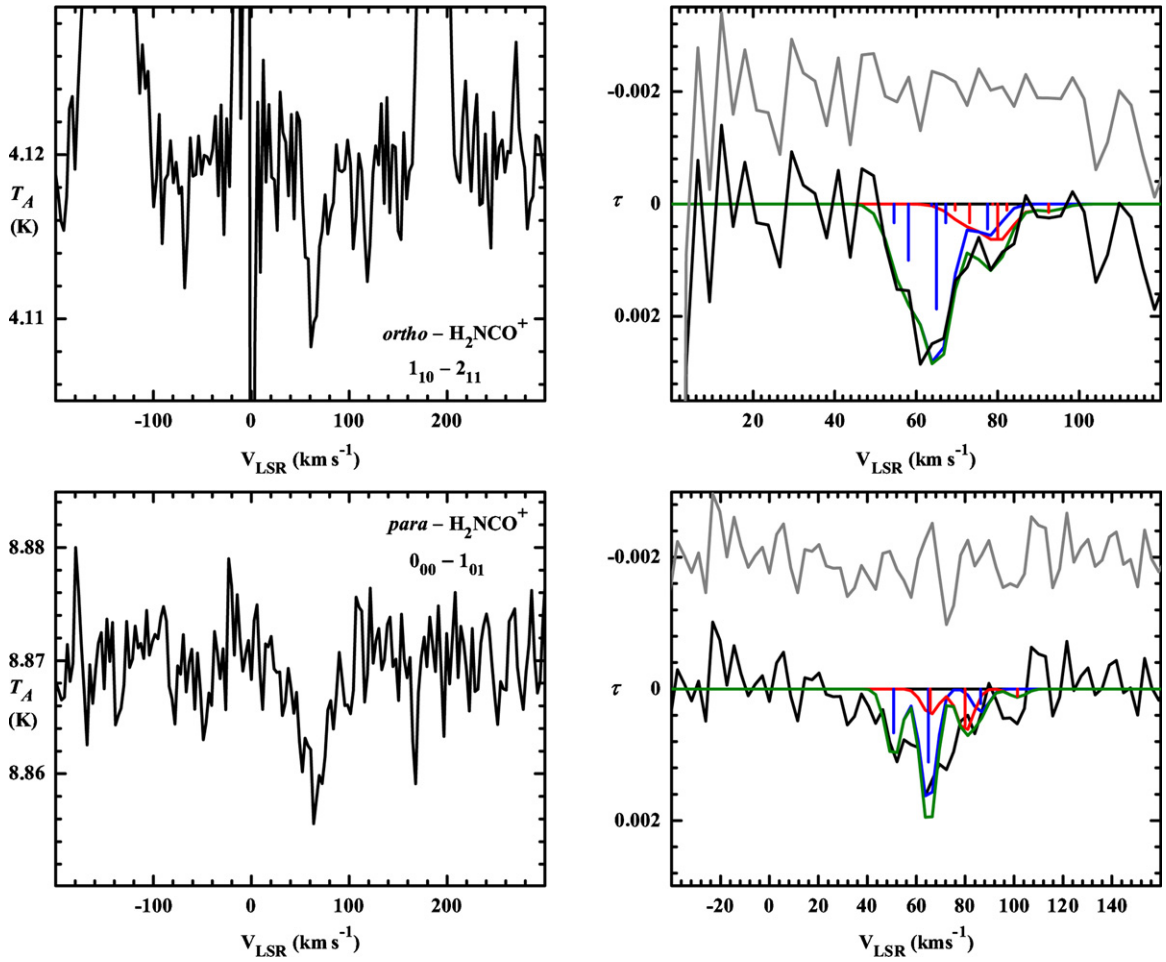

Figure 2. Absorption profiles of H_2NCO^+ observed toward Sgr B2(N) in the PRIMOS spectral line survey with the Green Bank Telescope. Left: raw position-switched spectra with the continuum from the background source indicated. Right: synthetic profiles at +65 km s^{-1} (red trace) and +80 km s^{-1} (blue trace), and the sum (green trace) overlaid on the observed profile (black trace). Shown in the same panels is the residual (gray trace) offset by −0.002 for clarity. The positions and relative intensities of the hfs components of the two kinematic components are indicated by the red and blue sticks. The spectrum of the $0_{0,0}$–$1_{0,1}$ transition was smoothed to an effective resolution of ∼2.9 km s^{-1} to coincide with that of the $1_{1,0}$–$2_{1,1}$ transition. The integration time was approximately 1 hr for the $0_{0,0}$–$1_{0,1}$ spectrum and 2 hr for the $1_{1,0}$–$2_{1,1}$ spectrum.

(A color version of this figure is available in the online journal.)

transitions in a near-prolate top. The sixth-order distortion constant H_{KJ} was included in the analysis, because tests on H_2CCO with a comparable set of rotational transitions to that in Table 1, showed that the rms is reduced by nearly 35% with the addition of this constant.

The derived spectroscopic constants in Table 2 are so accurate, that they allow the frequencies of the most important astronomical lines of H_2NCO^+ to be calculated to better than 3 parts in 10^7, or 0.1 km s^{-1} in equivalent radial velocity well into the far IR—i.e., adequate for most astronomical sources, including those with lines that are a fraction of a km s^{-1} wide. The initial measurements (Lattanzi et al. 2012) were of sufficient accuracy for an astronomical search in the centimeter band as this work shows, and the full set of spectroscopic constants obtained here should prove useful for future searches for H_2NCO^+ in the millimeter and far IR bands.

3. ASTRONOMICAL OBSERVATIONS OF H_2NCO^+

One of the most promising sources for H_2NCO^+ is Sgr B2, because the most intense lines of HNCO have been observed there. With accurate rest frequencies in hand, we examined published centimeter- and millimeter-wave spectra for evidence of H_2NCO^+ in this source (Cummins et al. 1986; Turner 1989; Remijan et al. 2008). On the assumption that the rotational temperature of H_2NCO^+ is comparable to that of HNCO ($T_{\rm rot} = 14^{+6}_{-4}$ K; Brünken et al. 2010), the most intense rotational lines would lie in the 2 and 3 mm bands, but unambiguous identification of lines of a new species in Sgr B2 is often unfeasible in these bands because of the high density of lines (spectral congestion). Not surprisingly, all but one of the principal transitions of H_2NCO^+ in the spectral line surveys in the 2 and 3 mm bands coincide with intense lines of other molecules. One exception is the $7_{0,7}$–$6_{0,6}$ transition near 141.6 GHz, but it was not detected at the level of sensitivity in the survey ($T_A < 10$ mK).

We then examined surveys in the centimeter band, because prior observations by several investigators have shown that spectral congestion is much lower at longer wavelengths. Two lines of H_2NCO^+ with $T_A \sim 10$ mK were tentatively identified in the PRIMOS[5] survey of Sgr B2(N) with the 100 m Green Bank Telescope (GBT): the lowest *para* transition ($0_{0,0}$–$1_{0,1}$) at 20.2 GHz and an *ortho* transition ($1_{1,0}$–$2_{1,1}$) at 40.8 GHz, both in

[5] http://www.cv.nrao.edu/∼aremijan/PRIMOS

Table 3
Lines of H_2NCO^+ Observed in Absorption toward Sgr B2(N)

Transition $J_{Ka,Kc}$–$J'_{K'a,K'c}$	Symmetry	Lab Freq.[a] (MHz)	V_{LSR} (km s^{-1})	S	E_l (K)	η_B	θ	$\int \tau dv$ (km s^{-1})	T_c (K)	N (10^{11} cm^{-2})
0_{00}–1_{01}	*Para*	20227.576(5)	64.5 ± 1.9	1.0	0.00	0.87	38″	0.032(10)	8.87	2–5
1_{10}–2_{11}	*Ortho*	40783.344(9)[b]	64.5 ± 1.5	1.5	0.02	0.63	19″	0.050(13)	4.12	4–9

Notes. Telescope pointing position was $\alpha(2000) = 17^h47^m19\overset{s}{.}8$, $\delta(2000) = -28°22'17''$. η_B is the antenna beam efficiency, and θ the beam width at FWHM. S is the line strength and E_l the energy of the lower level in the transition on the assumption of *ortho*/*para* symmetry. The column density (N) refers to either *ortho* or *para* H_2NCO^+.
[a] Frequencies used to derive the V_{LSR}. The frequencies were estimated from the peak intensities of synthetic profiles which are the superposition of the hyperfine components, each represented by a theoretical Gaussian profile with a FWHM of 7.7 km s^{-1}.
[b] The rest frequency of the underlying hyperfine split transition was calculated with the constants in Table 2.

absorption (Figure 2). Two other transitions were also covered in the PRIMOS survey ($1_{0,1}$–$2_{0,2}$ at 40.5 GHz and $1_{1,1}$–$2_{1,2}$ at 40.1 GHz), but the noise was too high to detect either transition ($T_A > 20$ mK).

There is evidence of underlying ^{14}N quadrupole hfs in both transitions in Sgr B2(N). From the laboratory measurements (Table 1), there are three hfs components for the $0_{0,0}$–$1_{0,1}$ transition with theoretical line strengths in the ratio 3:5:1 at the velocity offsets −14.2, 0, and +21.4 km s^{-1}. Similarly, there are six hfs components for the $1_{1,0}$–$2_{1,1}$ transition with line strengths of 15:45:1:84:15:20 at −10.4, −6.9, −1.2, 0, +2.2, and +12.5 km s^{-1}. The observed profiles (Figure 2) were simulated by representing each hyperfine component by a theoretical Gaussian profile whose relative intensity was constrained to the theoretical line strength, and the velocity and linewidth were constrained to those derived from recent observations of $^{13}CH^+$ and H_3O^+: V_{LSR} = +65 km s^{-1} and +80 km s^{-1} (Lis et al. 2012), and FWHM of 7.7 and 8.1 km s^{-1} (Godard et al. 2012). As Figure 2 shows, the sum of the simulated profiles for the two clouds at +65 and +80 km s^{-1} reproduces the observed profiles with only one free parameter (the optical depth).

Because the two lines are observed in absorption, the rotational temperature (T_{rot}) is less than the continuum temperature averaged over the antenna beam (T_c). For an optically thin absorption line (Liszt & Lucas 1995), the brightness temperature of the line (ΔT_B) in the Rayleigh–Jeans limit is

$$\Delta T_B = (T_A - T_c)/\eta_B \approx (T_{rot} - T_c/\eta_B - T_{CMB})\tau, \quad (1)$$

where η_B is the beam efficiency of the GBT (Table 3) and T_{CMB} = 2.73 K is the temperature of the cosmic microwave background. The antenna temperatures (T_A) and optical depths of the lines ($\tau \approx 1.8 \times 10^{-3}$ at 20.2 GHz and $\tau \approx 2.9 \times 10^{-3}$ at 40.8 GHz), imply that T_{rot} is comparable to or only a few degrees higher than T_{CMB}—i.e., 2.73K < T_{rot} < 4 K.

The two lines in Sgr B2(N) were assigned to H_2NCO^+ with great confidence because: (1) the astronomical frequencies are in excellent agreement with the laboratory frequencies to within 0.5 km s^{-1} or about 1/20 of the width of the astronomical lines; (2) both lines are observed in absorption with comparable optical depths; (3) the line widths are consistent with the underlying unresolved nitrogen–14 hfs; (4) the theoretical line profiles reproduce the observed profiles with only one free parameter (the optical depth for the kinematic components at +65 and +80 km s^{-1}); and (5) a misidentification is highly improbable, owing to the low density of absorption lines in Sgr B2(N) of about one line every 20 MHz—i.e., the probability that either line results from a chance coincidence to within a line width (Δv = 10 km s^{-1}) is $\leqslant 7 \times 10^{-2}$ and the joint probability for the two lines is $< 3 \times 10^{-3}$.

4. DISCUSSION AND CONCLUSIONS

The column density of H_2NCO^+ in the Sgr B2(N) halo was derived from the integrated optical depths of the two transitions in Table 3. The total column density of a molecular absorber is related to the integrated optical depth by the expression

$$N = \frac{3h}{8\pi^3 S\mu^2} \frac{Z}{1 - \exp(-h\nu/kT_{rot})} \int \tau dv, \quad (2)$$

where Z is the partition function at T_{rot}, S the line strength, μ the dipole moment, and ν the transition frequency. Owing to the low S/N and large overlap of the two kinematic components, the optical depth was integrated over the entire profile. On the assumption that 2.73 K < T_{rot} < 4 K (Section 3) and H_2NCO^+ has C_{2v} symmetry (see Section 2), N(para) = (6.6–16.3) × $10^{12} \int \tau dv$ and N(ortho) = (7.7–18.2) × $10^{12} \int \tau dv$ when evaluated explicitly at T_{rot} = 2.73 and 4 K. The total column density of H_2NCO^+ of (6 − 14) × 10^{11} cm^{-2} corresponds to a fractional abundance of $\sim 10^{-12}$, where $N(H_2) = 1 \times 10^{24}$ cm^{-2} (Lis & Goldsmith 1990).

The density is low in the region in Sgr B2(N) where H_2NCO^+ is observed. Surprisingly the rotational temperature (T_{rot}) is comparable to, or only slightly higher than, T_{CMB} (2.73 K; see Section 3) even though (1) σ, the cross-section for collisions of molecular ions with H_2, is large at low temperature; and (2) the critical density ($n_{critical}$) is very low, because the Einstein A for the two centimeter-wave lines are very small and therefore the collision rates are very low: $A = 5.5 \times 10^{-7}$ s^{-1} for the $0_{0,0}$–$1_{0,1}$ transition, and 4.0×10^{-6} s^{-1} for $1_{1,0}$–$2_{1,1}$. Similarly low rotational temperatures of only a few K have been derived from line of sight measurements of SH^+ and CH^+ toward Sgr B2(N) with *Herschel* (Godard et al. 2012). The rate coefficient $k(T)$ for collisions of HCO^+ with H_2 at temperatures below about 50 K (where $k(T) = \langle \sigma v \rangle$), is the benchmark measurement for a positive polyatomic molecular ion with H_2 (Pearson et al. 1995). On the assumption that $k(T)$ for H_2NCO^+ is comparable to that of HCO^+ (1.5×10^{-9} cm^3 s^{-1}; Pearson et al. 1995),[6] we estimate that $n(H_2)$ is $< 1 \times 10^4$ cm^{-3} in the region of the Sgr B2(N) halo where H_2NCO^+ is observed. Our estimate of $n(H_2)$ is similar to that derived from observations of HC_3N ($n(H_2)$ = (2–50) × 10^3 cm^{-3}; Morris et al. 1976) and HC_5N ($n(H_2)$ = (2–6) × 10^3 cm^{-3}; Avery et al. 1979) toward Sgr B2.

There is an intrinsic limitation in the interpretation of line of sight measurements toward distant objects in the galactic plane,

[6] To first order, the collisional rate coefficients $k(T)$ of singly charged ions with H_2 are similar, and depend only on the charge, average polarizabilty of H_2, and reduced mass of the collision-pair (Gioumousis & Stevenson 1958). Although σ is large at low temperatures, $k(T)$ remains constant with temperature (see Liao & Herbst 1996).

because molecular rotational lines may arise from the superposition of diffuse/translucent or dense gas (see Menten et al. 2011). As a result, it is difficult to determine the H_2NCO^+/HNCO ratio toward Sgr B2(N), and to characterize the molecular cloud(s) in which the H_2NCO^+ is observed. As expected from single antenna measurements, there is no direct information on whether H_2NCO^+ and HNCO are co-spatial, and in addition the $1_{0,1}$–$0_{0,0}$ and $2_{0,2}$–$1_{0,1}$ transitions of HNCO at 21.98 and 43.96 GHz are observed in emission in the PRIMOS survey rather than in absorption.

Lines of HNCO were observed in absorption in a far IR spectral line survey with *Herschel* by J. Neill et al. (in preparation). They derive a T_{rot} of 13 K and a column density of about 1×10^{15} cm^{-2} for the +64 km s^{-1} feature, implying that the H_2NCO^+/HNCO ratio in Sgr B2(N) is about 0.1%. However, it is unclear whether HNCO observed with *Herschel* is in the same region as that of H_2NCO^+ because: T_{rot} for HNCO is much higher, the energies of the upper levels are at least ten times higher than those of H_2NCO^+ and the critical densities are 10^3–10^4 times higher.

It is thought that H_2NCO^+ and $HNCOH^+$ are formed in the interstellar gas by proton transfer from H_3^+ to HNCO and HOCN, and hydrogen abstraction by $HNCO^+$ and $HOCN^+$ from H_2 (Marcelino et al. 2009; Quan et al. 2010). It is plausible that the formation of $HNCO^+$ and $HOCN^+$ is enhanced in less dense regions (e.g., the Sgr B2(N) halo), because: the NCO radical, which is thought to yield $HNCO^+$ and $HOCN^+$ by proton transfer, is calculated to have a high abundance per unit density in low to moderate density gas (Marcelino et al. 2009); and the cosmic-ray ionization rate and H_3^+ abundance per unit visual extinction are about an order of magnitude higher in regions with lower density (Indriolo & McCall 2012; Oka 2012).

A consistent picture of the chemistry of HNCO and its isomers will require further astronomical observations, gas kinetic measurements, theoretical calculations, and laboratory measurements including: (1) deep astronomical observations of $HNCOH^+$; (2) estimation of branching ratios inferred from $HNCOH^+$/HNCO, $HNCOH^+$/HOCN, and H_2NCO^+/HNCO abundances; (3) studies of H_2NCO^+ and $HNCOH^+$ in a range of objects, including GMCs and cold dark clouds; (4) observations of $HNCO^+$ and $HOCN^+$, the ionic precursors of protonated HNCO; (5) theoretical calculations and laboratory measurements of collisional rate coefficients; and (6) refinements in current gas phase chemical models.

Sgr B2 is the most prominent molecular cloud in the Central Molecular Zone (CMZ) of the Galaxy, but other clouds in the CMZ are also rich chemical repositories (Jones et al. 2012). Because HNCO has long been known to be widespread throughout the CMZ (Dahmen et al. 1997), and the highest abundances of H_3^+ have been observed there (Oka et al. 2005; Indriolo & McCall 2012), a search for H_2NCO^+ in other molecular clouds in the CMZ might be profitable. Absorption against continuum emission of other distant star-forming regions in the galactic plane may also be promising, because lines of sight toward these sources sample gas over a wide range of densities in the spiral arms, including dense gas in high-mass star-forming regions. Three new molecular ions (H_2O^+, HCl^+, and H_2Cl^+) in regions with low density were recently detected with *Herschel* at higher abundances than predicted (Gerin et al. 2012, and references therein), and OH^+ and SH^+ were detected in ground-based observations (Wyrowski et al. 2010; Menten et al. 2011). The observations here suggest that H_2NCO^+ also resides in a low-density region. Detection of other polyatomic ions with three heavy atoms, might confirm that the chemistry in less dense regions is much richer than previously supposed.

We are indebted to P. F. Goldsmith, M. Gerin, and D. C. Lis for helpful discussions; S. Thorwirth for communicating results of his high-level coupled cluster quantum calculations; J. Neill for sharing unpublished measurements of HNCO in Sgr B2(N) with *Herschel*; and F. Crim for advice and D. Kokkin for assistance with the preparation of the HNCO precursor in the laboratory experiments. The work in Cambridge was supported by NASA Grants NNX13AE59G, NNX08AE05G, and NNX08AI41G. A portion of this work was performed at the Jet Propulsion Laboratory, California Institute of Technology, under contract with the National Aeronautics and Space Administration.

REFERENCES

Adande, G. R., Halfen, D. T., Ziurys, L. M., Quan, D., & Herbst, E. 2010, ApJ, 725, 561
Avery, L. W., Oka, T., Broten, N. W., & MacLeod, J. M. 1979, ApJ, 231, 48
Brown, R. L. 1981, ApJL, 248, L119
Brünken, S., Belloche, A., Martín, S., Verheyen, L., & Menten, K. M. 2010, A&A, 516, A109
Brünken, S., Gottlieb, C. A., McCarthy, M. C., & Thaddeus, P. 2009, ApJ, 697, 880
Cummins, S. E., Linke, R. A., & Thaddeus, P. 1986, ApJS, 60, 819
Dahmen, G., Hüttemeister, S., Wilson, T. L., et al. 1997, A&AS, 126, 197
Gerin, M., Levrier, F., Falgarone, E., et al. 2012, RSPTA, 370, 5174
Gioumousis, G., & Stevenson, D. P. 1958, JChPh, 29, 294
Godard, B., Falgarone, E., Gerin, M., et al. 2012, A&A, 540, A87
Gottlieb, C. A., Myers, P. C., & Thaddeus, P. 2003, ApJ, 588, 655
Green, S. 1981, JPhCh, 85, 1676
Guarnieri, A., & Huckauf, A. 2003, Z. Naturforsch., 58a, 275
Hirota, T., Yamamoto, S., Mikami, H., & Ohishi, M. 1998, ApJ, 503, 717
Indriolo, N., & McCall, B. J. 2012, ApJ, 745, 91
Jones, P. A., Burton, M. G., Cunningham, M. R., et al. 2012, MNRAS, 419, 2961
Lattanzi, V., Thorwirth, S., Gottlieb, C. A., & McCarthy, M. C. 2012, J. Phys. Chem. Lett., 3, 3420
Liao, Q., & Herbst, E. 1996, JChPh, 104, 3956
Lis, D. C., & Goldsmith, P. F. 1990, ApJ, 356, 195
Lis, D. C., Schilke, P., Bergin, E. A., et al. 2012, RSPTA, 370, 5162
Liszt, H., & Lucas, R. 1995, A&A, 299, 847
Marcelino, N., Cernicharo, J., Tercero, B., & Roueff, E. 2009, ApJL, 690, L27
Marcelino, N., Brünken, S., Cernicharo, J., et al. 2010, A&A, 516, A105
Martín, S., Martín-Pintado, J., & Mauersberger, R. 2009, ApJ, 694, 610
Martín, S., Requena-Torres, M. A., Martín-Pintado, J., & Mauersberger, R. 2008, ApJ, 678, 245
Menten, K. M., Wyrowski, F., Belloche, A., et al. 2011, A&A, 525, A77
Morris, M., Turner, B. E., Palmer, P., & Zuckerman, B. 1976, ApJ, 205, 82
Oka, T. 2012, RSPTA, 370, 4991
Oka, T., Geballe, T. R., Goto, M., Usuda, T., & McCall, B. J. 2005, ApJ, 632, 882
Pearson, J. C., Oesterling, L. C., Herbst, E., & De Lucia, F. C. 1995, PhRvL, 75, 2940
Quan, D., Herbst, E., Osamura, Y., & Roueff, E. 2010, ApJ, 725, 2101
Remijan, A. J., Leigh, D. P., Markwick-Kemper, A. J., & Turner, B. E. 2008, arXiv:0802.2273
Snyder, L. E., & Buhl, D. 1972, ApJ, 177, 619
Tideswell, D. M., Fuller, G. A., Millar, T. J., & Marckwick, A. J. 2010, A&A, 510, A85
Turner, B. E. 1989, ApJS, 70, 539
Wyrowski, F., Menten, K. M., Güsten, R., & Belloche, A. 2010, A&A, 518, A26